Properties of Early Photolysis Intermediates of Rhodopsin Are Affected by Glycine 121 and Phenylalanine 261[†]

Stefan Jäger,[‡] May Han,[§] James W. Lewis,[‡] Istvan Szundi,[‡] Thomas P. Sakmar,[§,||] and David S. Kliger*[,‡]

Department of Chemistry and Biochemistry, University of California, Santa Cruz, California 95064, and Howard Hughes Medical Institute and Laboratory of Molecular Biology and Biochemistry, Rockefeller University, 1230 York Avenue, New York, New York 10021

Received May 13, 1997; Revised Manuscript Received July 21, 1997[⊗]

ABSTRACT: Glycine 121 in transmembrane (TM) helix 3 and phenylalanine 261 in TM helix 6 of bovine rhodopsin have been shown to be critical residues for creating an appropriate chromophore binding pocket for 11-*cis*-retinal [Han, M., Lin, S. W., Smith, S. O., and Sakmar, T. P. (1996) *J. Biol. Chem. 271*, 32330−32336; Han, M., Lin, S. W., Minkova, M., Smith, S. O., and Sakmar, T. P. (1996) *J. Biol. Chem. 271*, 32337−32342]. To further explore structure−function relationships in the vicinity of receptor helices 3 and 6, time-resolved absorption difference spectra of rhodopsin mutants G121A, G121V, and G121L/F261A were obtained at 20 °C. Data were collected from 30 ns to 690 ms after laser photolysis with 7 ns pulses ($\lambda_{max} = 477$ nm) and analyzed using a global exponential fitting procedure after singular value decomposition (SVD). For each mutant, the decay of its bathorhodopsin photoproduct (batho) into an equilibrium with its blue-shifted intermediate (bsi) was too fast to resolve (<20 ns). The reaction scheme found for the mutants G121A and G121L/F261A was batho/bsi → lumirhodopsin (lumi) → metarhodopsin I (MI) → metarhodopsin II (MII). For G121V, an additional early 380 nm absorber, with a back-reaction to lumi, had to be included in the above scheme. For the three Gly^{121} mutants, the main pathway to reach the active MII state is via lumi and MI. This is in contrast to rhodopsin where the main pathway in detergent samples is via lumi and an early 380 nm absorber, MI_{380}. From the accelerated batho decay present in all three mutants, we conclude that Gly^{121} is likely to participate in the earliest chromophore−protein interactions. In addition, bsi decay is further accelerated in mutant G121L/F261A, suggesting that Phe^{261} is an essential determinant of the protein processes involved in bsi decay.

Rhodopsin is a prototypical G protein-coupled heptahelical transmembrane (TM)[1] receptor (*1, 2*). It is locked into its inactive state by 11-*cis*-retinal, which is bound covalently to Lys^{296} (located in TM helix 7) via a protonated Schiff base (PSB). The counterion to the PSB has been identified as Glu^{113} (*3, 4, 5*) located in TM helix 3. Light-induced *cis*−*trans* isomerization transforms the retinal from the receptor antagonist to its agonist. The *trans* isomer remains covalently bound up to the metarhodopsin II (MII) state, the G protein-activating state of the receptor. Considerable progress has been made in relating retinal isomerization to receptor activation. To reach the G protein-activating state, R*, deprotonation of the Schiff base (SB) in rhodopsin is mandatory (*6*). The subsequent uptake of one proton from the aqueous phase (*7*) involving Glu^{134} at the cytoplasmic end of TM helix 3 (*8*) is also required. In an FTIR study, it has been shown that deprotonation of the SB is mechanistically coupled to protonation of the counterion Glu^{113} (*9*).

How are these electrostatic interactions related to the isomerization process of the retinal? Two independent studies, one involving site-specific spin-labels (*10*) and the other involving specific metal ion binding sites (*11*), both demonstrated that TM helices 3 and 6 move apart from each other upon MII formation. Recently it was suggested that these helix movements might originate in the chromophore movements of the early intermediates of rhodopsin (*12*). Specific chromophore features have been shown to be crucial in exerting steric effects on the protein in achieving the active state. Replacement of the β-ionone ring by two ethyl groups inhibited formation of MII and transducin activation (*13*), and removal of the C_9-methyl group reduced the G protein-activating capacity to 8% of that of rhodopsin (*14*).

In recent biochemical studies (*15, 16*), the authors showed that two specific sites, Gly^{121} on TM helix 3 and Phe^{261} on TM helix 6, play important roles in defining the 11-*cis*-retinal binding pocket of rhodopsin. Figure 1 shows the positions of Gly^{121} and Phe^{261} in a model of rhodopsin based on projection maps from Schertler and co-workers (*17, 18*) with assignments of the helices proposed by Baldwin (*19*). NMR constraints (*20*) were used to position the chromophore into its binding site (*11, 12*).

In the present study, we expand upon the biochemical studies (*15, 16*) by performing time-resolved UV−visible spectroscopy on the site-specific mutants G121A, G121V, and G121L/F261A. We show that the kinetics of the photoreactions and the λ_{max} values of the intermediates can be interpreted in terms of structural features of the chromophore binding pocket. The room temperature reaction

[†] This work was supported in part by NIH Grant EY00983 to D.S.K. T.P.S. is an Associate Investigator of the Howard Hughes Medical Institute. M.H. is a Charles H. Revson Fellow in Biomedical Research.

* To whom correspondence should be addressed.

[‡] University of California.

[§] Rockefeller University.

[||] Howard Hughes Medical Institute.

[⊗] Abstract published in *Advance ACS Abstracts,* September 15, 1997.

[1] Abbreviations: batho, bathorhodopsin; bsi, blue-shifted intermediate of rhodopsin; lumi, lumirhodopsin; meta I or MI or MI_{480}, metarhodopsin I; meta II or MII, metarhodopsin II; rho, rhodopsin; R*, activated form of rhodopsin; FTIR, Fourier-transform infrared; NMR, nuclear magnetic resonance; PSB, protonated Schiff base; SB, Schiff base; SVD, singular value decomposition; TM, transmembrane.

S0006-2960(97)01122-7 CCC: $14.00

Table 1: Summary of the λ_{max} Values and Shifts Relative to Parent Pigment Spectra (in Parentheses) in nm (Top Lines) and in cm^{-1} (Bottom Lines) of the Intermediates of Rhodopsin, Recombinant Rhodopsin (COS rho), and the Three Gly[121] Mutants[a]

species	rhodopsin[c]	COS rho[b]	G121A	G121V	G121L/F261A
pigment	498	500	498	477	487
	20080	20000	20080	20964	20534
batho	529 (+31)	531 (+31)	530 (+32)	507 (+30)	517 (+30)
	18904 (−1176)	18832 (−1168)	18868 (−1212)	19724 (−1240)	19342 (−1192)
bsi	477 (−21)	479 (−21)	456 (−42)	460 (−17)	462 (−25)
	20964 (+884)	20877 (+877)	21930 (+1850)	21739 (+775)	21645 (+1111)
lumi	492 (−6)	490 (−10)	482 (−16)	483 (+6)	477 (−10)
	20325 (+245)	20408 (+408)	20747 (+667)	20704 (−260)	20964 (+430)
MI_{480}	486[d] (−12)	NA	478 (−20)	479 (+2)	457 (−30)
	20576 (+496)		20920 (+840)	20877 (−87)	21882 (+1348)

[a] The estimated errors of λ_{max} values are ±2 nm, except for G121 batho intermediates where they are ±5 nm. Values in parentheses are spectral shifts of the intermediates relative to the dark state parent pigment spectra. [b] Values from (*32*). [c] Values from (*31*). [d] Value from (*23*). [e] NA, not applicable.

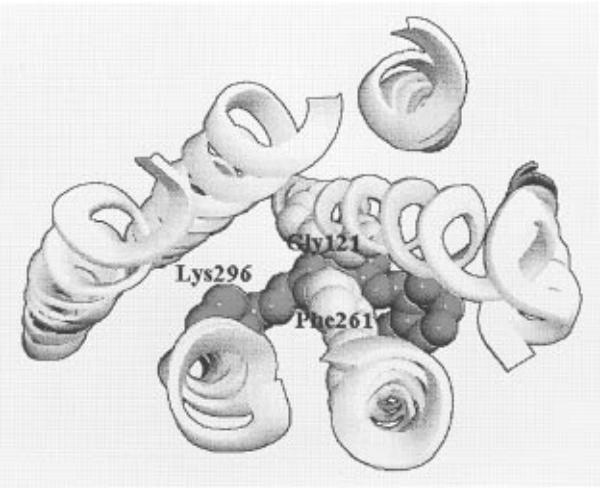

FIGURE 1: Model of bovine rhodopsin based on projection maps from Schertler and co-workers (*17*, *18*) with assignments of the helices from Baldwin (*19*). The view is perpendicular to the plane of the membrane from the cytoplasmic side to the intradiscal side. The locations of Gly[121] on TM helix 3 and Phe[261] on TM helix 6 are marked. Previous NMR data constrain the position of 11-*cis*-retinal (*20*). The figure was made with the same procedures as described in (*12*).

scheme leading to lumi formation for unmodified rhodopsin has been shown (Scheme 1) (*21*).

Scheme 1

$$\text{rho} \xrightarrow{h\nu} \text{batho} \rightleftharpoons \text{bsi} \rightarrow \text{lumi...}$$

The reaction scheme leading from lumi to MII is described most satisfactorily by Scheme 2 (*22*):

Scheme 2

$$\begin{array}{ccc} \text{...lumi} & \rightleftharpoons & MI_{380} \\ \downarrow & & \downarrow \\ MI_{480} & \rightleftharpoons & \text{MII} \end{array}$$

This scheme does not change when rhodopsin is solubilized in detergent (*23*). Here we show that the Gly[121] mutants studied follow different pathways in reaching the MII state than unmodified rhodopsin, and we use the kinetics to identify early steric trigger mechanisms that eventually lead to the active state of the receptor.

MATERIALS AND METHODS

Preparation of Rhodopsin Mutants. Opsin mutants G121A, G121V, and G121L/F261A were constructed and expressed in transiently transfected COS-1 cells as previously described (*15*, *16*). The resulting pigments were purified in dodecyl maltoside buffer solution [10 mM Tris-HCl, pH 7.0, 30 mM NaCl, 60 mM KCl, 2 mM $MgCl_2$, 0.1% (w/v) dodecyl maltoside] and concentrated as described previously (*24*, *25*).

Time-Resolved Spectroscopy. The photolysis measurements were performed in a microapparatus described previously (*26*). One microliter aliquots of pigment solution were photolyzed at 20 °C by 7 ns (fwhm), 80 $\mu J/mm^2$ pulses of 477 nm light from a Quanta Ray DCR-2 Nd:YAG pumped dye laser. The laser beam entered the sample at an angle of 90° from the probe beam, with vertical polarization. The probe beam polarization axis was set at magic angle (54.7°) with respect to the laser beam polarization to avoid kinetic artifacts due to rotational diffusion. The probe beam path length through the sample was 2 mm. After each laser pulse, the 1 μL sample was replaced by a flow system using a syringe whose plunger was controlled by a computer-driven stepper motor. Difference spectra were measured with a gated (20 ns) optical multichannel analyzer system as described previously (*27*, *28*). In order to determine absolute spectra of the photolysis intermediates, a photobleaching difference spectrum, from which the amount of rhodopsin bleached and the amount isorhodopsin formed by each laser pulse could be calculated, was obtained as described previously (*29*), with the bleach determined from the data collected at 690 ms in dodecyl maltoside buffer.

Data Analysis. All data analysis was performed by using global exponential fitting after singular value decomposition (SVD). The basic procedure has been described elsewhere (*22*, *30*, *31*), as were refinements used here (*32*). The entire set of absorbance data is fit at all wavelengths and delay times simultaneously. In the fitting procedure, the best fit was taken to be the one with the smallest number of exponentials giving reasonable residuals (actual data minus fit). The difference spectra corresponding to the wavelength-dependent amplitudes associated with the exponentials, called b-spectra, then were fit to kinetic schemes, resulting in λ_{max} values and microscopic lifetimes of the intermediates.

RESULTS

Rhodopsin mutants G121A, G121V, and G121L/F261A were regenerated with 11-*cis*-retinal and purified in detergent solution for spectral analysis. The λ_{max} values of the dark states of detergent-solubilized bovine rhodopsin, COS-cell rhodopsin, and the mutant pigments are listed in Table 1. Figure 2 shows the time-dependent absorption difference

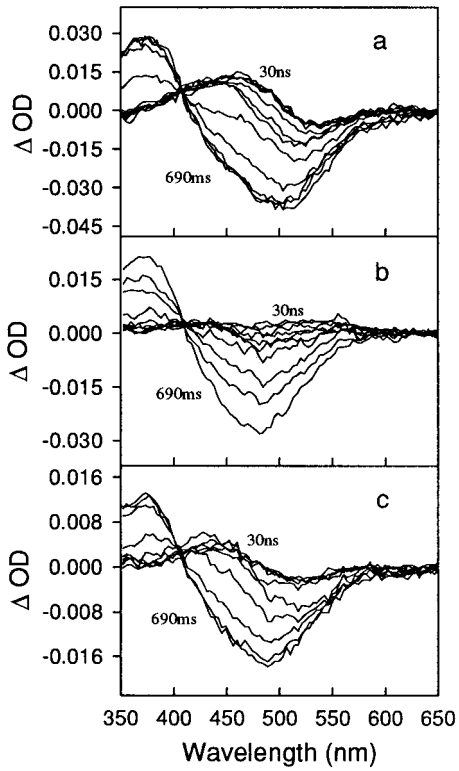

FIGURE 2: Absorption difference spectra for Gly^{121} mutants solubilized in dodecyl maltoside after photolysis with 7-ns (fwhm) 477-nm laser pulses at 20 °C, pH 7. Spectra were collected at various times. a: Mutant G121A measured at 30, 60, 120, 240, 480, and 960 ns; 10, 100, 250, and 500 μs; and 5 and 690 ms after photolysis. b: Mutant G121V measured at 30, 60, 120, 350, and 960 ns; 10, 30, and 100 μs; and 1 and 690 ms after photolysis. c: Double mutant G121L/F261A measured at 30, 60, 120, 350, and 960 ns; 10, 30, and 100 μs; and 1 and 690 ms after photolysis.

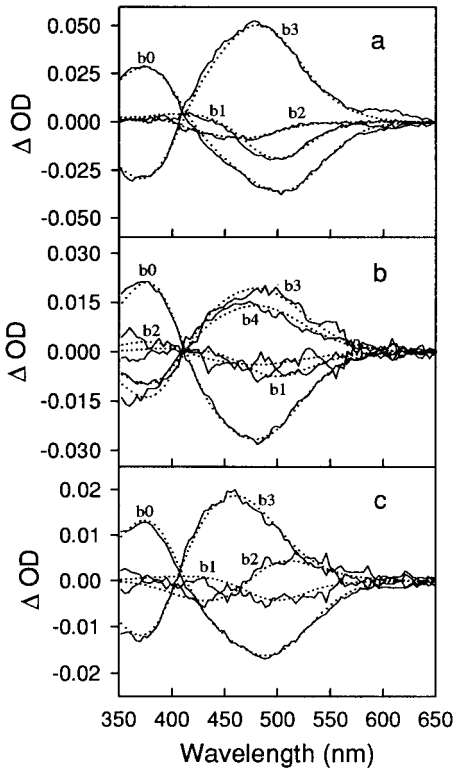

FIGURE 3: b-Spectra which resulted from multiexponential fits of data (noisy curves) and as deduced from corresponding fitted schemes (dotted curves). a: Mutant G121A resulted in a 3-exponential fit with time constants 100 ns, 14.0 μs, and 140 μs. b: Mutant G121V resulted in a 4-exponential fit with time constants 160 ns, 6.0 μs, 34.0 μs, and 2.0 ms. c: Double mutant G121L/F261A resulted in a 3-exponential fit with time constants 30 ns, 3.0 μs, and 60.0 μs.

spectra (intermediate − bleach) of the mutants G121A (Figure 2a), G121V (Figure 2b), and G121L/F261A (Figure 2c). At early times following pigment photolysis, the difference spectra clearly show that most of the batho has already decayed. The dominant intermediate for mutant G121A (Figure 2a) and G121L/F261A (Figure 2c) at early times is the blue-shifted intermediate, bsi. For G121V (Figure 2b), the λ_{max} shift of bsi relative to the parent pigment is less pronounced (see discussion below). The final product in all mutants is clearly a 380 nm absorber, most likely MII, since all photolyzed mutants show essentially normal ability to activate transducin (*15*, *16*).

Analysis of Mutant Pigment G121A. Replacing the residue Gly^{121} by Ala introduces one methyl group at the side chain position 121, which has almost no effect on the ground state absorbance with respect to the native pigment (*15*, Table 1). Figure 2a shows the difference spectra for times from 30 ns to 690 ms after photolysis. Analyzing the entire time range results in a 3-exponential fit with time constants $\tau_1 =$ 100 ns, $\tau_2 = 14.0$ μs, and $\tau_3 = 140$ μs. The corresponding difference spectra, called b-spectra, and the residuals (actual data minus fit) are shown in Figures 3a and 4a, respectively. The next step is to deduce which reaction scheme agrees with the b-spectra and their associated lifetimes. We were able to fit the b-spectra to the simplest scheme, a sequential scheme involving three lifetimes.

Scheme 3

$$\text{batho/bsi} \rightarrow \text{lumi} \rightarrow \text{MI} \rightarrow \text{MII}$$

In order to determine the initial amounts of batho and bsi, the first difference spectrum is decomposed assuming Gaussian shapes for the intermediate spectra. The best fit is represented by decomposing the 30 ns difference spectrum into 15% batho and 85% bsi (Figure 5a). This batho/bsi mixture decayed sequentially to lumi, MI, and finally to MII. The microscopic lifetimes of the photoproducts are summarized and compared to those of rhodopsin in Table 2. The decay of batho into an equilibrium with bsi was too fast to resolve (<20 ns), but the speed of bsi decay was comparable to what is observed in rhodopsin. The next intermediate, lumi, decays to MI (14.0 μs), which then decays to MII (140 μs). Measurements of COS-cell rhodopsin solubilized in detergent using the same amount of sample (300 μg) do not show the MI intermediate, but show instead the lumi intermediate decaying directly into MII (COS rho in Table 2: 310 μs), consistent with detergent strongly favoring the MII state. Essentially the same result is obtained for bovine rhodopsin solubilized in detergent (600 μs; Table 2). Only when measurements are made using milligram quantities and averaging over many difference spectra is it possible to observe additional processes in detergent, as shown from entries footnoted with *d* in Table 2. These measurements reveal that after lumi the reaction scheme branches off into 480 and 380 nm absorbers similar to MI_{480} and MI_{380} observed in membrane suspensions of rhodopsin. The 380 nm absorber is called MI_{380} to distinguish it from MII, which appears later, and the 480 nm absorber is called MI_{480} to distinguish it from MI_{380} (*22*). For rhodopsin in membrane, the data after lumi are adequately described by Scheme 2.

Table 2: Summary of the Decay Times of the Intermediates of Rhodopsin, COS-Cell Rhodopsin, and the Three Gly[121] Mutants[a]

species	rhodopsin	COS rho[b]	G121A	G121V	G121L/F261A
batho→BSI	74 ns[c]	100 ns	<20 ns	<20 ns	<20 ns
BSI→batho	107 ns[c]	190 ns			
BSI→lumi	105 ns[c]	190 ns	100 ns	260 ns	30 ns
lumi→BSI	none	none	none	400 ns	none
lumi→MI_{480}	2.1 ms[d]	NA	14.0 μs	600 μs	3.0 μs
lumi→MI_{380}	400 μs[d]	NA	NA	40.0 μs	NA
MI_{380}→lumi	312 μs[d]			60.0 μs	
MI_{380}→MII	333 μs[d]	NA	NA	none	NA
MI_{480}→MII	1.8 ms[d]	NA	140.0 μs	30.0 μs	60.0 μs
MII→MI_{480}	24.0 ms[d]		none	2.0 ms	none
lumi→MII	600 μs[b]	310 μs			

[a] The estimated errors of the decay times are 20%. [b] Values from (*32*). [c] Values from (*31*). [d] Values from (*23*). [e] NA, not applicable.

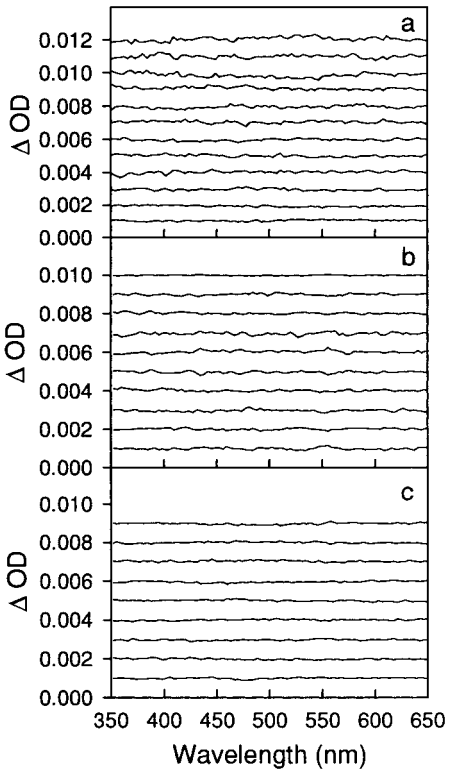

FIGURE 4: Residuals representing the actual data minus multiexponential fit. a: Mutant G121A. b: Mutant G121V. c: Double mutant G121L/F261A. The late times (upper traces) of panel a look more noisy, because less data per time point were recorded for mutant G121A at late times.

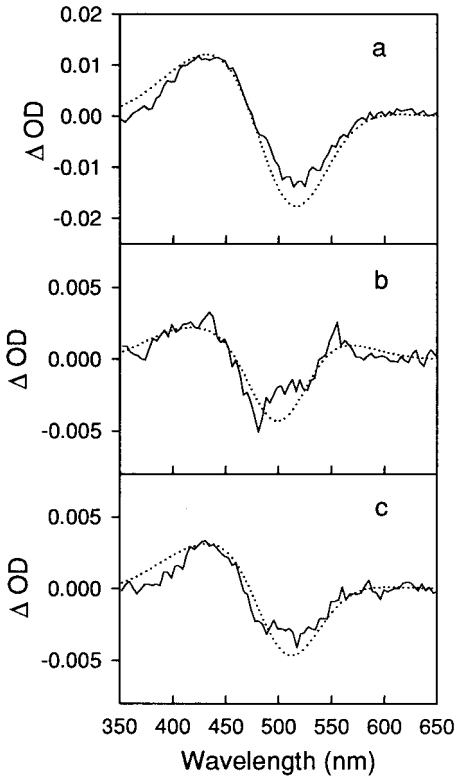

FIGURE 5: Absorption difference spectrum taken at 30 ns after photolysis (noisy curve) and calculated decomposition into batho, bsi, and bleach components (dotted curves). a: Mutant G121A. b: Mutant G121V. c: Double mutant G121L/F261A.

Recently it was shown that the same scheme applies for detergent-solubilized rhodopsin. However, the dominant pathway in detergent involves the direct decay of lumi into 380 nm absorbers: lumi → MI_{380} → MII (*23*; Table 2), making it more difficult to detect MI_{480}. Comparing the mutant G121A with the native pigment with respect to their speed of reaching the active MII state, the kinetics of the mutant are accelerated by a factor of 2−5 ($\approx 2k_bT$, which is small compared to the ΔG values involved in the transitions of the intermediates). From the kinetic scheme and the b-spectra, the intermediate − bleach spectra can be calculated and compared to the fit (Figure 6a). The λ_{max} values of the intermediates are summarized in Table 1 where the numbers in parentheses represent the λ_{max} shifts relative to the parent pigment spectrum. All of the MII intermediates absorbed at 380 nm and are not included in Table 1. The most striking feature of the mutant G121A is the more pronounced relative blue-shifts for the bsi, lumi, and MI spectra (numbers in parentheses in Table 1).

Analysis of Mutant Pigment G121V. In this mutant, the bulk introduced at position 121 is an isopropyl group. The ground state absorption spectrum of this mutant is shifted to 477 nm (*15*; Table 1). Figure 2b shows the difference spectra collected from 30 ns to 690 ms after photolysis. Analyzing the whole data set so that it satisfactorily minimizes the residuals (Figure 4b) requires a minimum of four exponentials to fit the data. The time constants are τ_1 = 160 ns, τ_2 = 6.0 μs, τ_3 = 34.0 μs, and τ_4 = 2.0 ms, and the corresponding b-spectra are shown in Figure 3b. The b-spectra and corresponding time constants were fit best by Scheme 4.

Scheme 4

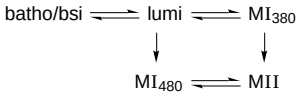

The initial amounts of batho and bsi present in the 30 ns difference spectrum were calculated to be 20% and 80%,

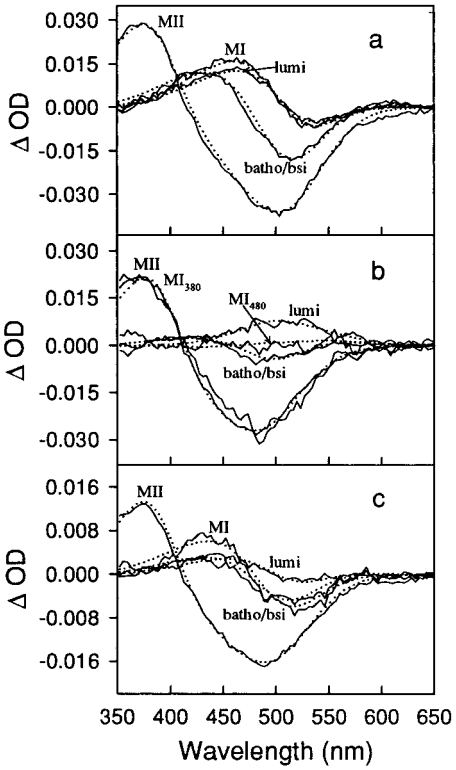

FIGURE 6: Intermediate minus bleach spectra (noisy curves) calculated from the b-spectra (Figure 3, noisy curves) and the microscopic lifetimes. The fits (dotted curves) represent the Gaussian shape of the intermediate difference spectra. The λ_{max} values and the decay constants from the fits are summarized in Tables 1 and 2, respectively. a: Mutant G121A. b: Mutant G121V. c: Double mutant G121L/F261A.

respectively (Figure 5b). This batho/bsi mixture is in equilibrium with lumi and subsequently branches off into an early 380 nm absorber and MI (which now is called MI_{480}). The dominant pathway to reach the active MII state is via lumi and MI_{480}, as observed for mutant G121A. All the microscopic lifetimes are summarized in Table 2. The major difference between mutant G121V and mutant G121A is that the batho/bsi mixture is in equilibrium with lumi and that MI_{480} is in equilibrium with MII. The observations that (1) batho, bsi, and lumi are all in equilibrium with each other, (2) batho/bsi decays more slowly than in the other mutants, and (3) the relative blue-shift of G121V bsi is reduced (relative to its parent pigment, see below) account for the different shapes of the difference spectra at early times (Figure 2b).

The intermediate − bleach spectra calculated from the scheme and the b-spectra are shown in Figure 6b. The λ_{max} values of the intermediates are summarized in Table 1. The most striking feature of Table 1 is that lumi and MI_{480} are slightly red-shifted relative to the parent pigment while they are blue-shifted in rhodopsin and mutant G121A (numbers in parentheses in Table 1).

Analysis of Mutant Pigment G121L/F261A. Introducing Leu instead of Gly at position 121 adds more bulk than introduced in the two previous mutants. To compensate for this steric effect on TM helix 3, bulk was reduced at position 261 in TM helix 6 (Phe was replaced by Ala). This "rescue" mutation has been found to partially compensate for the blue-shift of the dark state absorption (Table 1) and for biochemical effects resulting from the introduction of a bulky side chain at position 121 (*16*). Figure 2c shows the difference spectra for times from 30 ns to 690 ms after photolysis. Analyzing the entire time range results in a 3-exponential fit with time constants $\tau_1 = 30$ ns, $\tau_2 = 3.0$ μs, and $\tau_3 = 60.0$ μs. The corresponding b-spectra and the residuals are shown in Figures 3c and 4c, respectively, and the b-spectra could be fit to Scheme 3.

The decomposition of the 30 ns difference spectrum resulted in 10% batho and 90% bsi (Figure 5c). As for mutant G121A, this batho/bsi mixture decayed in a sequential manner to lumi and then to MI and MII. The microscopic lifetimes are summarized in Table 2. Again, batho decaying into an equilibrium with bsi was too fast to resolve (<20 ns). The subsequent decay of bsi (30 ns) is accelerated by a factor of 3−6 compared to rhodopsin. The next intermediate, lumi, decayed to MI (3 μs), which then decayed to MII (60 μs). Thus, the appearance of the active MII species is accelerated by a factor of 5−10 compared to rhodopsin. From the kinetic scheme and the b-spectra, the intermediate − bleach spectra were calculated (Figure 6c). The λ_{max} values of the intermediates are summarized in Table 1. The relative blue-shifts of bsi and lumi (numbers in parentheses) are comparable to rhodopsin, while MI exhibits a much more pronounced blue-shift.

DISCUSSION

In a mutagenesis study of rhodopsin, Han et al. showed that substitutions of Gly^{121} with amino acids containing progressively larger side chains caused a progressive blue-shift in the λ_{max} value of the pigment, a decrease in thermal stability, an increase in reactivity with hydroxylamine, and a relative reversal in the selectivity of opsin for 11-*cis*-retinal over *all-trans*-retinal (*15*). They also showed that the loss of function phenotypes of the Gly^{121} mutations could be partially reversed by specifically replacing Phe^{261} by alanine as a second site mutation. It was concluded that Gly^{121} on TM helix 3 and Phe^{261} on TM helix 6 formed part of the retinal binding pocket responsible for receptor activation (*16*). These findings motivated us to look for differences in the early trigger mechanisms in the photoactivation of the mutant pigments G121A, G121V, and G121L/F261A by rapid time-resolved spectroscopy.

Structural Model for the Chromophore Pocket. In mutant G121A, the ground state absorption spectrum was minimally affected, but a susceptibility to hydroxylamine attack in the dark and an increased transducin activating capacity of the mutant opsin incubated with *all-trans*-retinal were observed (*15*). These findings were strong evidence for a significant change in the structure of the chromophore pocket, even for the Gly^{121} mutant with the smallest structural change (G121A). Combining the results of the Gly^{121} and Phe^{261} mutations with NMR data, the authors of a recent study (*11*) modeled the retinal binding site and suggested that the C_9-methyl group of the retinal is oriented to be in van der Waals contact with Gly^{121} on TM helix 3. Phe^{261} on TM helix 6 was suggested to be located in close proximity (but not in direct van der Waals contact) to Gly^{121}, the interaction being established most likely via contacts to the retinal. Increasing bulk at position Gly^{121} was suggested to result in an outward movement of helix 3. Rigid body movements of helices 3 and 6 relative to each other, which must result in an increase in the distance between Gly^{121} and Phe^{261}, were reported to

be a major feature in reaching the active state of the receptor (*10*, *33*). In a modeling study which combined time-resolved linear dichroism data (*34*) with time-resolved UV−vis spectroscopy of Schiff base counterion mutants (*32*), the movements of the chromophore from batho to lumi within the chromophore pocket have been deduced (*12*). In the transition to lumi, the chromophore moves toward helix 3, which could start the outward movement of helix 3 in this intermediate. An increase in volume (∼29 cm^3/mol) accompanying lumi formation is consistent with this picture (*35*). In the modeling study (*11*), the authors suggested that the ring portion of the retinal maintains its close proximity to helix 3 in the subsequent MI intermediate. The following discussion interprets the reaction kinetics and λ_{max} shifts found for the three mutants G121A, G121V, and G121L/F261A in the context of this emerging picture of the molecular mechanism of receptor activation.

Kinetics of the Mutant Photointermediates. In the mutants studied, batho decay into an equilibrium with bsi was too fast to resolve (<20 ns). Thus, the introduction of even a relatively small group such as a methyl group at position 121 changes the structure of the chromophore pocket enough to strongly affect the stabilities of the early photointermediates. The highly distorted chromophore in batho, which is thought to represent the main energy storage via chromophore−protein interactions (*20*, *36*, *37*), is relaxed much faster. Since it has been shown that batho decay depends on a rotational barrier in the C_6-C_7 bond of the chromophore, which results from steric interaction between the C_5-methyl group and C_8-H (*21*, *38*), it is most likely that it is the ring end of the chromophore that interacts differently with the chromophore pocket. The mutations studied here affect batho decay in two ways, first accelerating the rate and second forward-shifting the equilibrium with bsi. Both these effects could result from Gly^{121} mutations increasing the volume of the chromophore pocket. A volume increase could lower the barrier to bsi formation by increasing ring flexibility, which has been previously shown to lower this barrier (*38*). An increase in volume also could forward-shift the equilibrium with bsi, since retinal analogs with added bulk which crowd the pocket display back-shifted equilibrium constants (*21*). In this picture, the outward movement of helix 3 by the Gly^{121} mutations would lower both the enthalpy of the batho/bsi barrier and the enthalpy of the bsi intermediate.

The decay rate of the batho/bsi mixture for the single mutants does not change by more than a factor of 2 compared to rhodopsin (Table 2). It is interesting to note that all pigments with artificial retinals investigated in (*39*) showed the same effect. It was concluded that bsi decay depends on specific protein features rather than chromophore features. The fact that bsi decay was speeded up substantially (∼5 times) in G121L/F261A shows that Phe^{261} is involved in the protein interactions responsible for bsi decay. The interaction between Phe^{261} and the chromophore in bsi could be reduced due to the shortening of the side chain at position 261 in mutant G121L/F261A. This interpretation is consistent with the chromophore motion described in (*12*) where the ring portion of the chromophore moves toward helix 6 in the transition from batho to bsi and away from helix 6 in the transition from bsi to lumi.

Lumi in all mutants investigated decayed via MI_{480} to MII, in contrast to the case in detergent solubilized rhodopsin where the dominant pathway is through an early 380 nm absorbing species (MI_{380}) (*23*). It has been suggested that protein conformational changes leading to Schiff base deprotonation are driven by steric interactions, while Schiff base deprotonation and subsequent changes are driven by electrostatic interactions (*11*). The results for the mutants studied here are consistent with this picture in that the bulky substituents at 121 dramatically speed up MI_{480} formation, a step immediately preceding Schiff base deprotonation. Since all Gly^{121} mutants reacted with hydroxylamine in the dark (*15*), changes in the counterion environment must already be present in the dark state and obviously persist at least until MII is reached.

Lumi decay into MI for mutant G121V was 40 × and 200 × slower than for mutant G121A and mutant G121L/F261A, respectively. Since there was no reaction observed for MI_{380} to MII in mutant G121V, the main pathway to reach the active MII state is via MI_{480}. It takes 4 × or 33 × longer to reach MII for mutant G121V than for mutant G121A or mutant G121L/F261A, respectively. This can be seen by comparing τ_3 for mutant G121A (140 μs) and mutant G121L/F261A (60 μs) with τ_4 of mutant G121V (2.0 ms). Thus, the "rescue" mutant G121L/F261A could compensate for the slowed down kinetics in mutant G121V and establish a value for MII appearance close to the value obtained for G121A. The fact that the kinetic schemes found for mutants G121A and G121L/F261A are the same (Scheme 3) but different from the scheme found for mutant G121V (Scheme 4) shows that molecular engineering can reverse a change originally imposed on the system by mutagenesis. The change in this case is represented by substituting Ala^{121} for Val^{121} (helix 3), and the reversing change is represented by further substituting Phe^{261} for Ala^{261} (helix 6). However, the original rhodopsin state could never be reestablished by any of the double replacement mutants (*16*). In particular, the accessibility for hydroxylamine in the dark persisted for all Gly^{121} mutants.

In a previous time-resolved spectroscopy study on Schiff base counterion mutants, different reaction schemes were found for different mutations. The salient result from all mutants investigated so far by time-resolved spectroscopy (*32* and herein) is that all mutants followed the general Scheme 5. Different protein environments such as the native membrane versus detergent micelles, or site-directed mutagenesis, merely emphasize different pathways or change the kinetics within the general scheme.

Scheme 5

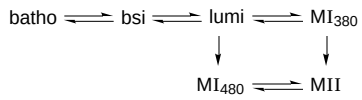

Spectral Shifts of the Mutant Photointermediates. Despite different λ_{max} values for the ground state absorbance, similar batho red-shifts relative to the parent pigment spectra were observed for all mutants studied [numbers in parentheses of Table 1; since there is very little batho present (10−20%) at the first time point investigated, the shifts have a large error (±5 nm)]. If we assume that the chromophore binding pockets for all mutants studied differ in the ground state, it is likely that in batho they differ as well. The accelerated batho decay (Table 2) suggests a less pronounced chromophore−protein interaction in the mutant pigments investigated.

In the transition to bsi, where relaxation of the chromophore twists mainly occurs, the relative blue-shifts are clearly different for all mutants (numbers in parentheses of Table 1). Comparing the relative bsi blue-shifts of rhodopsin and the mutants G121A and G121V, it is clear that increasing bulkiness at position 121 does not simply add up to an increased relative blue-shift in bsi. The opposite is the case (less blue-shift for G121V bsi than for G121A bsi). This shows that there are at least two factors contributing to the spectral shifts. We speculate that the spectral shifts past batho may involve at least a combination of (1) the distance between the retinal ring and Glu^{122}, and (2) a change in orientation of the retinal ring.

It is also worthwhile considering the absolute λ_{max} values of bsi and lumi in all three mutants. Both values do not differ by more than ±3 nm among the mutants, in contrast to the relative shifts, which differ much more (numbers in parentheses). This suggests that once a bulky group is introduced at position 121 the general features for bsi and lumi remain the same regardless of variations in the corresponding mutations. This is consistent with the kinetic results, where batho decay is speeded up for all Gly^{121} mutants. The most puzzling result is the relatively large blue-shift for G121L/F261A MI. Whereas the absolute value for the λ_{max} of MI is near 480 nm for rhodopsin, G121A, and G121V, the value for G121L/F261A is ~20 nm more shifted to the blue. If Gly^{121} is in van der Waals contact with the chromophore (C_9-methyl group) (*11*) and addition of bulk at position 121 in the form of alanine or valine did not change the absolute λ_{max} value of MI absorption, it is hard to imagine that leucine would blue-shift MI by 20 nm. We therefore conclude that Phe^{261} is responsible for the blue-shift.

Conclusion. Time-resolved UV−visible spectroscopy involving rhodopsin mutants with substitutions in the chromophore pocket is particularly useful for deducing detailed structural information related to chromophore motion (*12*, *32*). In the present study, we have specified the effects of amino acids Gly^{121} and Phe^{261} which were determined to involve the specific transitions batho to bsi, and bsi to lumi, respectively. The kinetic data suggest both amino acids are likely to participate in the steric trigger mechanisms. Ongoing work may eventually lead to a better understanding of the characteristics of the chromophore binding pocket that control the primary events of coupling the light signal of retinal isomerization to receptor activation.

REFERENCES

1. Stryer, L. (1986) *Annu. Rev. Neurosci. 9*, 87−119.
2. Stryer, L. (1991) *J. Biol. Chem. 266*, 10711−10714.
3. Sakmar, T. P., Franke, R. R., and Khorana, H. G. (1989) *Proc. Natl. Acad. Sci. U.S.A. 86*, 8309−8313.
4. Zhukovsky, E. A., and Oprian, D. D. (1989) *Science 246*, 928−930.
5. Nathans, J. (1990) *Biochemistry 29*, 9746−9752.
6. Longstaff, C., Calhoon, R. D., and Rando, R. R. (1986) *Proc. Natl. Acad. Sci. U.S.A. 83*, 4209−4213.
7. Arnis, S., and Hofmann, K. P. (1993) *Proc. Natl. Acad. Sci. U.S.A. 90*, 7849−7853.
8. Arnis, S., Fahmy, K., Hofmann, K. P., and Sakmar, T. P. (1994) *J. Biol. Chem. 269*, 23879−23881.
9. Jäger, F., Fahmy, K., Sakmar, T. P., and Siebert, F. (1994) *Biochemistry 33*, 10878−10882.
10. Farrens, D. L., Altenbach, C., Yang, K., Hubbell, W. L., and Khorana, H. G. (1996) *Science 274*, 768−770.
11. Shieh, T., Han, M., Sakmar, T. P., and Smith, S. O. (1997) *J. Mol. Biol. 269*, 373−384.
12. Jäger, S., Lewis, J. W., Zvyaga, T. A., Szundi, I., Sakmar, T. P., and Kliger, D. S. (1997) *Proc. Natl. Acad. Sci. U.S.A. 94*, 8557−8562.
13. Jäger, F., Jäger, S., Kräutle, O., Friedman, N., Sheves, M., Hofmann, K. P., and Siebert, F. (1994) *Biochemistry 33*, 7389−7397.
14. Ganter, U. M., Schmid, E. D., Perez-Sala, D., Rando, R. R., and Siebert, F. (1989) *Biochemistry 28*, 5954−5962.
15. Han, M., Lin, S. W., Smith, S. O., and Sakmar, T. P. (1996) *J. Biol. Chem. 271*, 32330−32336.
16. Han, M., Lin, S. W., Minkova, M., Smith, S. O., and Sakmar, T. P. (1996) *J. Biol. Chem. 271*, 32337−32342.
17. Schertler, G. F. X., Villa, C., and Henderson, R. (1993) *Nature 362*, 770−772.
18. Schertler, G. F. X., and Hargrave, P. A. (1995) *Proc. Natl. Acad. Sci. U.S.A. 92*, 11578−11582.
19. Baldwin, J. M. (1993) *EMBO J. 12*, 1693−1703.
20. Han, M., and Smith, S. O. (1995) *Biochemistry 34*, 1425−1432.
21. Kliger, D. S., and Lewis, J. W. (1995) *Isr. J. Chem. 35*, 289−307.
22. Thorgeirsson, T. E., Lewis, J. W., Wallace-Williams, S. E., and Kliger, D. S. (1993) *Biochemistry 32*, 13861−13872.
23. Mah, T. L., Szundi, I., Lewis, J. W., Jäger, S., and Kliger, D. S. (1997) *J. Biol. Chem.* (submitted for publication).
24. Fahmy, K., and Sakmar, T. P. (1993) *Biochemistry 32*, 9165−9177.
25. Zvyaga, T. A., Fahmy, K., and Sakmar, T. P. (1994) *Biochemistry 33*, 9753−9761.
26. Lewis, J. W., and Kliger, D. S. (1993) *Rev. Sci. Instrum. 64*, 2828−2833.
27. Einterz, C. M., Lewis, J. W., and Kliger, D. S. (1987) *Proc. Natl. Acad. Sci. U.S.A. 84*, 3699−3703.
28. Lewis, J. W., Warner, J., Einterz, C. M., and Kliger, D. S. (1987) *Rev. Sci. Instrum. 58*, 945−949.
29. Albeck, A., Friedman, N., Ottolenghi, M., Sheves, M., Einterz, C. M., Hug, S. J., Lewis, J. W., and Kliger, D. S. (1989) *Biophys. J. 55*, 233−241.
30. Szundi, I., Lewis, J. W., and Kliger, D. S. (1997) *Biophys. J. 73*, 688−702.
31. Hug, S. J., Lewis, J. W., Einterz, C. M., Thorgeirsson, T. E., and Kliger, D. S. (1990) *Biochemistry 29*, 1475−1485.
32. Jäger, S., Lewis, J. W., Zvyaga, T. A., Szundi, I., Sakmar, T. P., and Kliger, D. S. (1997) *Biochemistry 36*, 1999−2009.
33. Sheikh, S. P., Zvyaga, T. A., Lichtarge, O., Sakmar, T. P., and Bourne, H. R. (1996) *Nature 383*, 347−349.
34. Lewis, J. W., Einterz, C. M., Hug, S. J., and Kliger, D. S. (1989) *Biophys. J. 56*, 1101−1111.
35. Marr, K., and Peters, K. S. (1991) *Biochemistry 30*, 1254−1258.
36. Birge, R. R., Einterz, C. M., Knapp, H. M., and Murray, L. P. (1988) *Biophys. J. 53*, 367−385.
37. Smith, S. O., Courtin, J., de Groot, H., Gebhard, R., and Lugtenburg, J. (1991) B*iochemistry 30*, 7409−7415.
38. Mah, T. L., Lewis, J. W., Sheves, M., Ottolenghi, M., and Kliger, D. S. (1995) *Photochem. Photobiol. 62*, 356−360.
39. Randall, C. E., Lewis, J. W., Hug, S. J., Björling, S. C., Eisner-Shanas, I., Friedman, N., Ottolenghi, M., Sheves, M., and Kliger, D. S. (1991) *J. Am. Chem. Soc. 113*, 3473−3485.

BI971122F